PCCP

Accepted Manuscript

ROYAL SOCIETY OF CHEMISTRY

www.rsc.org/pccp

Competition between H_2O and $(H_2O)_2$ reactions with CH_2OO/CH_3CHOO

Liang-Chun Lin[1,2], Hung-Tzu Chang[1], Chien-Hsun Chang[1], Wen Chao[1,2], Mica C. Smith[1,3], Chun-Hung Chang[1], Jim Jr-Min Lin[1,2], Kaito Takahashi[1]**

[1] Institute of Atomic and Molecular Science, Academia Sinica, Taipei 10617, Taiwan

[2] Department of Chemistry, National Taiwan University, Taipei 10617, Taiwan

[3] Department of Chemistry, University of California, Berkeley, Berkeley, CA 94720, USA

AUTHOR INFORMATION

Corresponding Author

*kt@gate.sinica.edu.tw, jimlin@gate.sinica.edu.tw

ABSTRACT

In this study, we performed *ab initio* calculations and obtained the bimolecular rate coefficients for the CH_2OO/CH_3CHOO reactions with $H_2O/(H_2O)_2$. The energies were calculated with QCISD(T)/CBS//B3LYP/6-311+G(2d,2p) and the partition functions were estimated with anharmonic vibrational corrections by using the second order perturbation theory. Furthermore, we directly measured the rate of CH_2OO reaction with water vapor at high temperatures (348 and 358 K) to reveal the contribution of water monomer in the CH_2OO decay kinetics. We found that the theoretical rate coefficients reproduce the experimental results of CH_2OO for a wide range of

temperatures. For *anti*- (*syn*-) CH_3CHOO, we obtained theoretical rate coefficients of 1.60×10^{-11} (2.56×10^{-14}) and 3.40×10^{-14} (1.98×10^{-19}) cm^3 sec^{-1} for water dimer and monomer reactions at room temperature. From the detailed analysis on the quantum chemistry and approximations for the thermochemistry calculation, we conclude that our calculated values should be within a factor of 3 of the correct values. Furthermore, at $[H_2O]=1\times10^{17}$ to 5×10^{17} cm^{-3}, we estimate that the effective first-order rate coefficients for CH_2OO, *anti*- and *syn*-CH_3CHOO reactions with water vapor will be ~10^3, ~10^4, and ~10^1 s^{-1}, respectively. Thereby, for Criegee intermediates (CIs) with a hydrogen atom on the same side as the terminal oxygen atom, the reaction with water vapor will likely dominate the removal processes of these CIs in the atmosphere.

TOPIC GRAPHICS

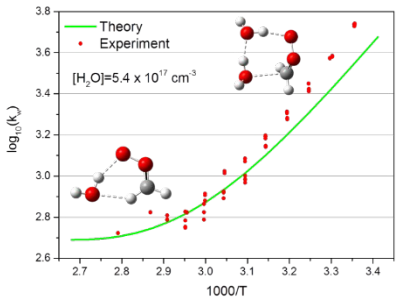

KEYWORDS

Atmospheric chemistry, rate coefficient, transient absorption, quantum chemistry, anharmonic correction

Introduction

Due to their possible participation as active oxidants in the troposphere, carbonyl oxides, also called as Criegee intermediates (CIs)[1] have been of great interest in atmospheric studies.[2–4] These CIs are formed in the troposphere by ozonolysis of unsaturated hydrocarbons. Due to its very high reactivity, it is very hard to quantify their concentrations in the atmosphere. Presently there are no methods to measure the concentration of a CI in the atmosphere, and the only way to know the concentration is through the rates of its production and removal. Recently, an efficient method to generate stable CIs in the laboratory was developed by Taatjes and coworkers.[5,6] This has allowed direct experimental determination of bimolecular rate coefficients for CIs with atmospheric trace gas species[7–12] and has initiated several theoretical[13–18] and modelling[19,20] studies. Considering that the water concentration in the troposphere is much higher than other trace gases that can react with CIs such as SO_2 and NO_2, it is important to quantify the absolute reaction rate with water vapor.[21–25] Indeed, pioneering theoretical works on the CI water reactions were performed by Ariya's group[26–28] as well as by Anglada's group[29–32] nearly ten years ago. However, their theoretical rate coefficients for the anti-$CH_3CHOO+H_2O$ reaction at room temperature vary by two orders of magnitude: 6.7×10^{-16} (Ariya's group[27]) versus 1.7×10^{-13} (Angleada's group[32]) cm^3 sec^{-1}. The difference in the rate coefficients was attributed to the different quantum chemistry methods used for the energetics.[32]

Our previous experimental study has shown that the water dimer reaction with CH_2OO dominates the decay kinetics of CH_2OO at room temperature and the bimolecular reaction rate coefficient of $CH_2OO+(H_2O)_2$ is 7.4×10^{-12} cm^3 sec^{-1} at room temperature.[33,34] In addition, an ozonolysis experiment (which used a different source for the water dimer equilibrium constants) has recently reported a value of $\sim1.1\times10^{-11}$ cm^3 sec^{-1} at 293 K.[23] Furthermore, this water dimer

reaction has a very strong temperature dependence, our experimental rate coefficient decreases by a factor of 3 when temperature is raised from 5 to 50 °C.[34] Accordingly, thermochemistry calculation with *ab initio* energetics and frequencies showed a negative activation energy of ~ -8 kcal mol^{-1}, consistent with the experimental observations. At room temperature, because the water dimer reaction is very fast at typical humidity levels, the water monomer reaction can be significant only at very low humidity. An experimental rate coefficient of CH_2OO with water monomer has been reported to be 3.2×10^{-16} cm^3 sec^{-1} for $[H_2O] <10^{15}$ cm^{-3}.[24] On the other hand, Ouyang et al.[25] and Stone et al.[11]reported much smaller values of 9.0×10^{-17} cm^3 sec^{-1} and 2.5×10^{-17} cm^3 sec^{-1} at much higher water concentrations.

Once a hydrogen atom is substituted by a methyl group to make CH_3CHOO, *anti* and *syn*-conformers are present due to the position of the CH_3 with respect to the OO bond. Furthermore, as highlighted by the conformer specific detection by Taatjes and coworkers[7] as well as by Lee and coworkers,[9] the reaction rate with SO_2/NO_2 is sensitive to the location of the methyl group. Water vapor kinetic experiments were conducted by Taatjes et al. as well as by Sheps et al.; and they reported rate coefficients of *anti*-$CH_3CHOO+H_2O$ reaction to be 1.0×10^{-14} and 2.4×10^{-14} cm^3sec^{-1}, respectively at 298 K. On the other hand, the *syn*-$CH_3CHOO+H_2O$ reaction was reported to be slower than their detection limit.[7,12] These experimental values are in between the values calculated by Ariya's group[27] (6.7×10^{-16} cm^3sec^{-1}) and by Anglada's group[32] (1.7×10^{-13} cm^3sec^{-1}). Previous theoretical studies by Ariya's group have predicted water dimer reaction to have room temperature bimolecular rate coefficients of 3.8×10^{-12} cm^3sec^{-1} and 2.2×10^{-15} cm^3sec^{-1} for *anti*- and *syn*-CH_3CHOO, respectively.[28] However to the best of our knowledge, there are no experimental reports on the values for the water dimer reaction. In addition, there are no studies

discussing the temperature dependence, as well as the competition of the water monomer and water dimer rates as a function of temperature at water concentrations relevant to atmospheric conditions.

In this study we performed theoretical simulation using high level quantum chemistry methods including anharmonic vibrational correction to calculate the bimolecular rate coefficients of CH_2OO, and *anti*-/*syn*-CH_3CHOO reactions with water monomer and dimer. Furthermore, by improving our previous set up, we obtained the experimental values at higher temperatures (348 and 358 K) for the kinetics of CH_2OO reaction with water vapor. For CH_2OO, we compared our theoretical results with experimental results to provide understanding on the general temperature dependence of the effective rate with water vapor. The rest of the paper is organized in the following manner. In section 2, the details for the experimental and theoretical methods will be given. In section 3, we present detailed analysis of the theoretical calculations and compare them with available experimental results. Lastly we provide a brief conclusion with atmospheric implications of our study in section 4.

Experimental and theoretical methods

1. Experimental Methods

The experimental apparatus has been described previously.[33,34] CH_2OO was prepared via the well-established reaction of $CH_2I + O_2 \rightarrow CH_2OO + I$. The carrier gas N_2 was mixed with water vapor, O_2, and CH_2I_2 vapor in Teflon tubes upstream of the reactor and the gas mixture entered the reactor through an inlet at the center and exited to the vacuum pump through outlets at both ends of the reactor. The reaction took place in the flow cell where the total pressure was controlled at 300 Torr with 10 Torr oxygen. CH_2OO was generated from photolysis of the gaseous mixture at 248 nm (KrF excimer laser) via reaction between O_2 and CH_2I radical, which was generated by laser photolysis of CH_2I_2. The CH_2I_2 vapor was obtained by flowing the buffer gas above CH_2I_2

liquid which was slightly heated (~7 K above room temperature, to improve the stability of the vapor concentration). Water vapor was introduced into the reactor by passing a portion of the carrier gas over a heated water surface to produce the desired relative humidity. All the gas flows were controlled by mass flow controllers (Brooks, 5850E or 5800E). Flow rates were adjusted to fully refresh the gas in the reactor between 1 Hz photolysis pulses. Small streams of N_2 gas (~5% of the total flow) were used to purge the windows.

The photolysis reactor was immersed in a circulating water bath which was connected to a temperature-controlled water circulator (Yih Der BL-730, stability ±0.1 K). The temperature of the reactor was measured with 3 resistance temperature detectors (RTDs, Newport Omega, F2020-1000-A) located in glass wells near the center and the two ends of the reactor. The reactor gas temperature under typical experimental conditions was calibrated against the temperature readings with a Rotronic temperature and humidity sensor (Rotronic, HC2-S; 0.1-0.2 K temperature accuracy; 0.8% relative humidity accuracy at 298 K, 1.8% above 333 K) placed inside the reactor at different water bath temperatures and different sensor locations before the experiment. (This Rotronic sensor was removed for the kinetic measurements.) The measured temperature stability was better than ±0.3 K (with accuracy better than ±0.6 K) for all experiments. The reactant gas mixture and purge gas were preheated to the water bath temperature in copper tubes upstream of the reactor. Error estimates for the water concentration is given in the electronic supplementary information (ESI).

Transient absorption signal of the reaction system was measured with a continuous broadband light source (Energetiq, EQ-99), a balanced photodiode detector (Thorlabs, PDB450A) and a band-pass filter at 340 nm (Edmund Optics 65129, 10 nm OD4 band pass filter). The light source was projected to the entrance of the photolysis tube (25 mm inner diameter, 76 cm long) by an

achromatic lens (Thorlabs ACA254-100-UV). To enhance the absorption signal, the probe light was reflected 8 times through the photolysis reactor by a spherical mirror (R = 1 m, Thorlabs, CM750-500-F01) and a SiO_2 prism. The probe beam and the photolysis beam were overlapped collinearly in the photolysis reactor.

A small time-dependent transmittance change (< 1%) was observed after the photolysis pulse even without adding any sample. This background did not depend on the water concentration and can be subtracted by performing a background run under the same experimental condition except adding CH_2I_2. The presented data are after the background subtraction.

2. Theoretical methods

The stationary points for CH_2OO, CH_3CHOO, H_2O, $(H_2O)_2$, and their van der Waals (VDW) complex $CH_2OO\cdots H_2O$, $CH_3CHOO\cdots H_2O$, $CH_2OO\cdots(H_2O)_2$, and $CH_3CHOO\cdots(H_2O)_2$ were all optimized by B3LYP[35,36]/6-311+G(2d,2p)[37,38] for their singlet ground electronic states. Next, we determined the transition state (TS) structures for the lowest energy paths of the formation of hydroxylalkyl hydroperoxide, $CH_2(OH)OOH$, and $CH_3CH(OH)OOH$ for CH_2OO and *anti*-/*syn*-CH_3CHOO, respectively. To quantify the minima (transition state) geometries, we performed frequency calculations and confirmed that there were zero (one) imaginary frequencies. For the transition states we performed intrinsic reaction path calculation to confirm the reactants and the products for the reaction. Furthermore, anharmonic vibrational calculation, using the vibrational second order perturbation theory (VPT2), was performed at these geometries.[39,40] The B3LYP calculations were all performed using the Gaussian09 program[41] with "opt=verytight", "integral=ultrafine" and "freq=anharmonic" keywords for the VPT2 calculation. All the geometries are given in the ESI. Using these B3LYP geometries, we performed complete basis set (CBS) extrapolation[42] using Dunning's aug-cc-pVDZ, aug-cc-pVTZ, and aug-cc-pVQZ[43–45]

basis sets with quadratic configuration interaction singles and doubles with perturbative triples (QCISD(T))[46]; and coupled cluster singles and doubles with perturbative triples (CCSD(T))[47]. The Hartree Fock energy was extrapolated using the $E_{CBS} + \mathrm{Ae}^{-\mathrm{BX}}$ while the correlation energy was extrapolated using $E_{CBS} + \mathrm{Ae}^{-(X-1)} + \mathrm{Be}^{-(X-1)^2}$ where X is the cardinal number of the basis set and E_{CBS}, A, B are optimization parameters. In order to confirm the validity of the energetics given by the single reference methods, we also performed multireference configuration interaction and multireference perturbation theory calculation, CASPT2, using the B3LYP geometries for a selected reaction path of $CH_2OO\cdots H_2O$. For the multireference calculations, we used 10 orbitals 10 electrons active space, and more details are given in the ESI. Furthermore, the B3LYP geometries were compared with those obtained by the optimization using QCISD(T)/aug-cc-pVTZ for selected reaction paths of $CH_2OO\cdots H_2O$ and $CH_2OO\cdots(H_2O)_2$. All QCISD(T), CCSD(T), as well as multireference methods were performed using the MOLPRO program.[48] Energies will be reported in kcal mol^{-1}, where 1 kcal mol^{-1}= 4.184 kJ mol^{-1}.

Considering the contribution of water monomer reaction and water dimer reaction, the effective reaction rate of CI with water vapor can be written as

$$\frac{-d[CI]}{dt} = \left\{\sum_i k_{mono,i}[H_2O] + \sum_j k_{dimer,j}K_{eq,H_2O}[H_2O]^2\right\}[CI] = k_w[CI] \qquad (1)$$

where k_{mono} and k_{dimer} are the bimolecular rate coefficients of CI with water and water dimer, respectively. For the water dimer concentration, in order to stay consistent with our previous experimental studies[33,34], we used the equilibrium constant values given by Ruscic[49] to obtain the water dimer concentration by $[(H_2O)_2] = K_{eq,H2O}[H_2O]^2$. The summation of i and j corresponds to the number of independent reaction paths that are possible for water and water dimer, respectively.

The calculation of the k_{mono} and k_{dimer} was performed assuming thermal equilibrium between the reactants and the VDW complex as well as the steady state approximation for the activated complex. Therefore, the bimolecular rate constant is obtained from the equilibrium constant (K_{eq}) between the reactants (CI+H_2O or CI+$(H_2O)_2$) and the VDW complex; and the unimolecular rate coefficient of the VDW complex (k_{VDW}) forming the product using transition state theory. Therefore the bimolecular rate coefficients are given as

$$k(T) = K_{eq}(T)\kappa(T)k_{VDW}(T) \quad (2)$$

where the tunneling correction, κ, is estimated using the semiclassical approximation of Miller's group.[50,51] The temperature dependent K_{eq} and k_{VDW} were calculated using the THERMO, ADENSUM, LAMM, and SCTST programs in the Multiwell suite[52–55]. Lastly, previous work by Ariya and coworkers has shown that contribution from the larger water clusters will be several orders smaller than the dimer contribution, so we ignored the contribution from larger clusters, such as water trimer, in the present study[28].

Results and Discussions

1. Experimental Results

The representative transient absorption traces of CH_2I_2/O_2 photolysis system under various humidity levels at 358 K are shown in Figure 1. The decay of CH_2OO at dry condition ([H_2O] < 1×10^{16} cm^{-3}) is primarily due to CH_2OO reaction with radical species including I atoms, CH_2IOO and CH_2OO; reaction with water vapor dominates the observe decay under wet conditions. Clear exponential decay of the transient absorption of CH_2OO was observed, suggesting that the depletion of CH_2OO can be described by the formula below.

$$-\frac{d[CH_2OO]}{dt} = k_{obs}[CH_2OO] = k_0[CH_2OO] + k_w[CH_2OO] \quad (3)$$

Here k_{obs} is the observed rate constant obtained from the exponential decay and we assume k_{obs} to be the sum of the dry loss rate k_0 and the loss rate due to reaction with water vapor k_w. This k_w corresponds to the effective rate of water reaction given in eq (1). After subtracting k_0 from k_{obs}, we plot k_w with respect to the water concentration in Figure 2.

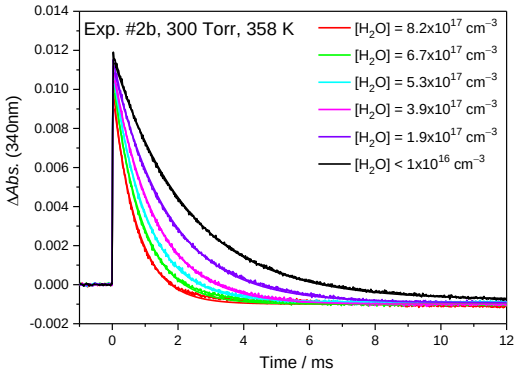

Fig. 1 Representative time traces of CH_2OO decay under different water concentrations at 358 K (Exp. #2b, see Table S1). A rapid increase in absorption after the photolysis laser pulse at time = 0 corresponds to the formation of CH_2OO, which absorbs very strongly at 340 nm; the negative baseline at long time is caused by the depletion of the precursor, CH_2I_2, which absorbs weakly at 340 nm.[33,34] The smooth lines are the single exponential fit to the data.

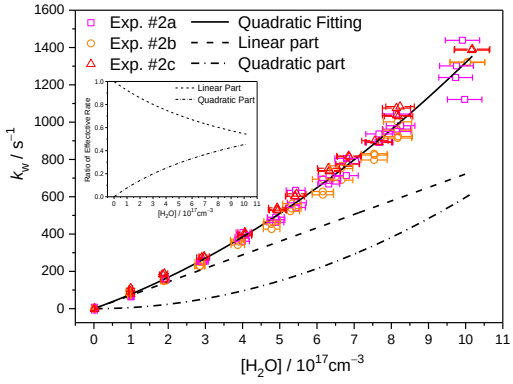

Fig. 2 Pseudo-first-order rate coefficient of CH_2OO loss plotted against water concentration at 358 K. The solid curve is a polynomial fit (including linear and quadratic terms) to the data. The dash

line shows the contribution of the linear term; the dash-dotted curve is the contribution of the quadratic term. The relative contributions of these two terms are shown in the inset. The horizontal error bars indicate the estimated errors in [H_2O] (see ESI). The standard deviations of the fitted rate coefficients may represent the vertical error bars, but they are too small to see.

Figure 2 shows the pseudo-first-order effective rate coefficients of the CH_2OO loss ($k_w = k_{obs} - k_0$) due to reaction with water vapor at 358 K. A polynomial is used to fit the data as a function of [H_2O]. At this temperature, adding a linear term of [H_2O] is necessary to fit the experimental data, suggesting the contribution of the water monomer reaction. We obtain 7.3×10^{-16} and 6.8×10^{-13} cm^3 sec^{-1} for the monomer and dimer rate constant at 358K. This is very different from the case at lower temperatures, where a pure quadratic function was enough to obtain a good fit, indicating that the water monomer reaction is insignificant at low temperature. Figure 3 shows the pseudo-first-order rate coefficient of CH_2OO reaction with water vapor as well as their polynomial fit at temperatures from 283 to 358 K. The experimental bimolecular rates extracted from these fits are given in Table S1, and compared with theoretical values in the following sections.

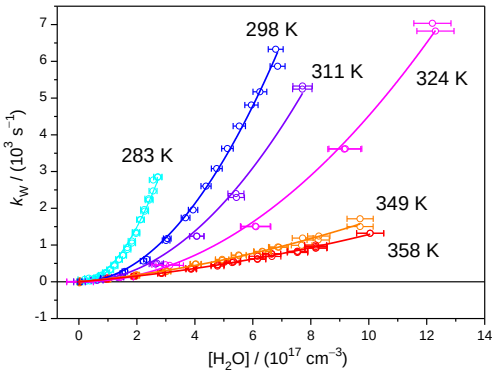

Fig. 3 Pseudo-first-order CH_2OO loss rate coefficients k_w plotted against H_2O concentration. The curves for 324 K and lower temperatures are pure quadratic fits to the data, which are adapted from reference 34. For experiments at 349 and 358 K, an additional linear term is necessary to fit the

data satisfactorily. The horizontal error bars indicate the estimated errors in [H_2O] (see ESI). The standard deviations of the fitted rate coefficients may represent the vertical error bars, but they are too small to see.

2. Quantum chemistry results for CH_2OO

We located 2 reaction paths for the CI+H_2O reaction, and 4 reaction paths for the CI+$(H_2O)_2$ reaction using B3LYP/6-311+G(2d,2p). We use 1a, 1b to label the two water monomer reaction paths while 2a, 2b, 2c, 2d will be used for the water dimer reaction. The new reaction paths found in our study is related to the geometries previously reported by Ariya's group:[26,27] 2a and 2b through the rotation of the free OH bonds of the water molecule in the complex. (see ESI for more details concerning the geometrical differences from previous works). We believe that we have an extensive collection of reaction paths to properly describe the reactions of CI with water vapor to form hydroxyalkyl hydroperoxide. The relative energy diagram for the water vapor reactions with CH_2OO is given in Figure 4. For the CH_2OO+H_2O reaction, there is also a hydrogen transfer reaction forming HCOOH as reported by Nakajima et al.[56] as well as by Crehuet et al.[29] However, the TS energy is too high (11.3 kcal mol^{-1} compared to the reactant, calculated at QCISD(T)/CBS//B3LYP/6-311+G(2d,2p)) to compete with the reaction making $HOCH_2OOH$. Therefore we did not consider this hydrogen transfer pathway in the present study.

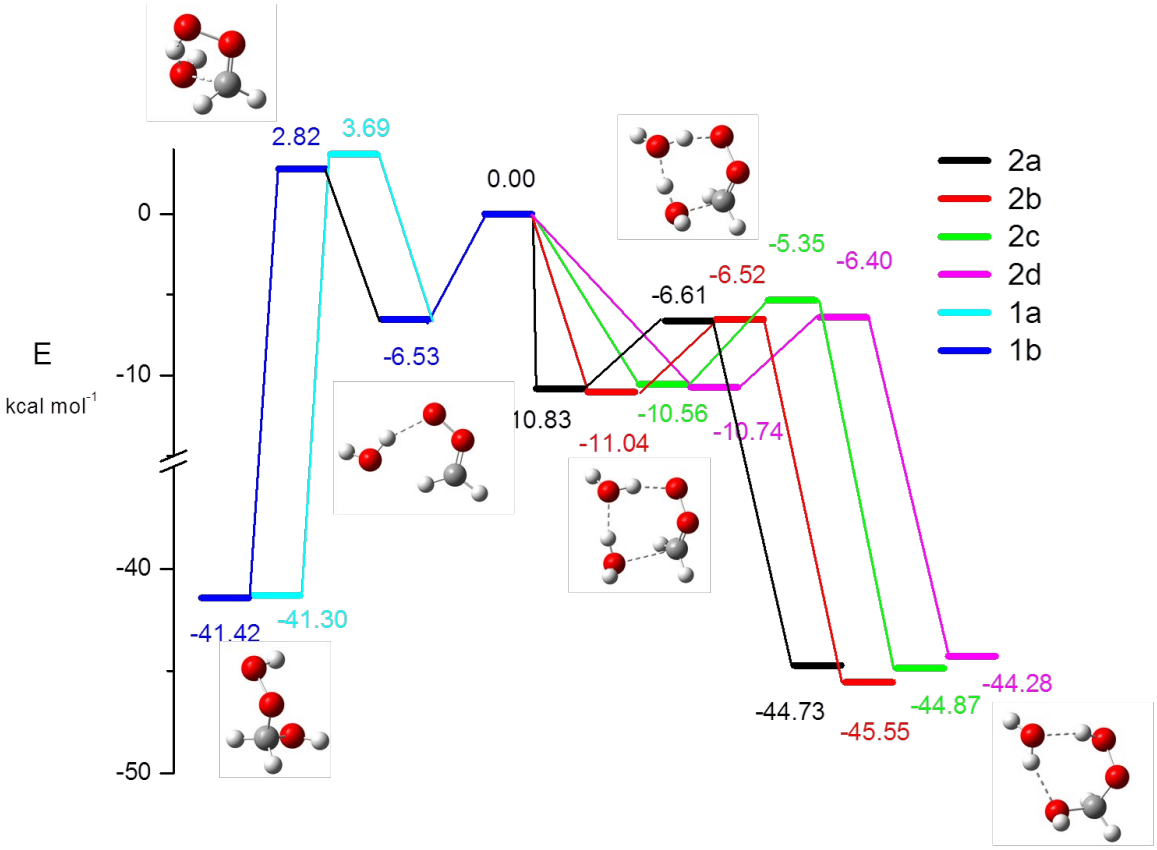

Fig. 4 Potential energy diagram for the reactions of $CH_2OO + H_2O$ (left) and $CH_2OO + (H_2O)_2$ (right). Energetics are calculated using the electronic energies by QCISD(T)/CBS//B3LYP/6-311+G(2d,2p), and vibrational zero-point correction by B3LYP/6-311+G(2d,2p). Schematic structures for the 1b and 2a pathways are also given.

In Table 1, we compare the zero-point-corrected energies obtained from the different quantum chemistry methods for the 1b water monomer and the 2a water dimer reactions. We list the energetics for all 6 pathways in Table S2. One can notice that there is ~ 1 kcal mol^{-1} CBS correction to the QCISD(T)/aug-cc-pVTZ results for the barrier energy (the energy difference between the VDW minima and TS). Accordingly, our TS energies with respect to the reactant are slightly higher than those obtained by Angelada and coworkers[26] for the water monomer

reaction which were obtained at the CCSD(T)/aug-cc-pVTZ level. We also compared the CBS limit energies of QCISD(T) versus those of CCSD(T) and as given in Table S4, they were all within ~0.2 kcal mol^{-1} from each other except for the product exothermicity. Due to the zwitterionic and diradical characters of CH_2OO, one may wonder the validity of the single reference methods.[57–59] Indeed the T1 diagnostic[60] values for the VDW complex with CCSD(T) and QCSISD(T) were ~0.05, which are larger than the accepted value for closed shell systems. On the other hand, the TS had a much smaller T1 diagnostic value of ~0.025. Thereby, we have also performed single-point calculation using multireference calculation for the 1b reaction path using (at the B3LYP geometries, see Table S3 of ESI). The calculated barrier energies by the multireference methods were only 0.3 kcal mol^{-1} higher than the QCISD(T) results. Therefore, although CH_2OO is a multireference system, the cluster expansion and configuration interaction methods are able to recover most of static correlation energies. This has been confirmed by Anglada and coworkers[61] as well as by Vereecken and Fransisco[14] in other CI systems. In addition, for the carbonyl oxide isomer of CH_2OO, Miliordos et al. have recently mentioned that biradical characteristic is not large.[62]

Next, one may question the validity of the B3LYP/6-311+G(2d,2p) geometries, therefore, we also performed geometry optimization for the VDW, TS and product for 1a 1b and 2a reaction path using QCISD(T)/aug-cc-pVTZ. We found that bonds length for B3LYP are within 0.01 Å of QCISD(T) and the bond angles were within 10°. Furthermore, when we compared the optimized QCISD(T)/aug-cc-pVTZ energies with the QCISD(T)/aug-cc-pVTZ single point energies calculated at the B3LYP geometries, the barrier energies were within 0.2 kcal mol^{-1} of each other. From these detailed evaluation, (see ESI Tables S2-S6) we conclude that the electronic energy error for the CI+H_2O/$(H_2O)_2$ reactions is within 0.5 kcal mol^{-1}. However we note that this is an

optimistic estimate since other systems, such as CH_2OO+O_3 reaction, have had larger variation in the energetics with different quantum chemistry methods[18]. The CBS extrapolation using more accurate CCSD(T)-F12 methods, used in the CH_2OO+O_3 study, or multireference methods with larger active space may clarify the error more but it is beyond the scope of this paper.

As shown in Table 1, all methods show a similar trend that the monomer has a complex forming energy of ~6 kcal mol^{-1} while the dimer complex is formed by a stabilization of ~11 kcal mol^{-1}. Consistent with previous studies[28,32], the monomer complex is formed by the water donating a hydrogen bond to the oxygen of CH_2OO and accepting a hydrogen bond from the CH bond of CH_2OO. This is seen from the intermolecular bond distance of 1.87 and 2.13 Å for $HOH\cdots OOCH_2$ and $OOHCH..OH_2$, respectively. To form $CH_2(OH)OOH$, the water oxygen has to move greatly to approach the carbon atom of CH_2OO. On the other hand, the oxygen atom of the second water in the VDW complexes (2a, 2b, 2c, 2d) is at a favorable geometry to approach the carbon atom on CH_2OO. Therefore, while the barrier energies for the monomer reaction are ~9 kcal mol^{-1}, those for the dimer reaction drop to ~4 kcal mol^{-1}. As a result, the TS energies are below the reactants' energy for the dimer reaction, while they are positive for the monomer reaction.

Table 1 Vibrational zero-point-corrected energies, in kcal mol^{-1}, for the 2a dimer and 1b monomer reaction paths for the three systems: CH_2OO, *anti*-CH_3CHOO, and *syn*-CH_3CHOO with three different quantum chemistry methods. The zero of energy is the reactants, $CI+H_2O$ or $CI+(H_2O)_2$. All the calculation are at the geometries optimized by B3LYP/6311+G(2d,2p).

	B3LYP/6-311+G(2d,2p)			QCISD(T)/AVTZ			QCISD(T)/CBS		
Structure	vdw	ts	prd	vdw	ts	prd	vdw	ts	prd
				CH_2OO					
2a	-10.63	-7.96	-41.15	-11.56	-8.04	-45.29	-10.83	-6.61	-44.73
1b	-6.13	2.37	-38.55	-6.80	1.83	-41.73	-6.53	2.82	-41.42
				anti-CH_3CHOO					

2a	-12.38	-6.91	-36.93	-14.46	-9.21	-43.81	-13.72	-7.47	-43.08
1b	-7.13	1.25	-34.39	-8.40	-0.85	-40.35	-8.03	0.34	-39.88
				syn-CH_3CHOO					
2a	-10.50	-2.99	-32.99	-12.56	-5.07	-39.22	-11.84	-3.18	-38.44
1b	-6.26	7.56	-30.65	-7.35	5.68	-35.76	-6.91	6.96	-35.24

3. Bimolecular reaction rates of CH_2OO with water and water dimer

In Figure 5, we present the Arrhenius plots of the bimolecular rate coefficients of CH_2OO reactions with H_2O and $(H_2O)_2$ using three approaches: 1. rigid rotor harmonic oscillation approximation (RRHO); 2. VPT2 anharmonic approximation (VPT2) and 3. VPT2 anharmonic corrections with hindered rotor approximation (VPT2+HR), as well as the available experimental values. The final approach was used only for the dimer reaction, and our present dimer results are slightly different from those reported previously[34]. This is because we only considered the internal rotation of the water dimer in the previous study, while in the present study we also considered the internal rotation for the $CH_2OO(H_2O)_2$ VDW complex and TS. Furthermore, we previously used anharmonic VPT2 values at geometries obtained with normal optimization criteria, which resulted in inaccurate values for the low frequency vibration. In the present case, we used a more stringent optimization criteria. For the RRHO and VPT2 schemes, we consider that these paths are all independent and the total rate coefficient is given as the sum of the four independent paths.

All rate coefficients could be fit to the Arrhenius form of $A\exp(-E_a/RT)$ and we obtained $2.88 \times 10^{-17}\exp(7.87/RT)$, $7.08 \times 10^{-18}\exp(8.03/RT)$, and $4.11 \times 10^{-18}\exp(8.08/RT)$ for the dimer reaction with RRHO, VPT2 and VPT2-HR, respectively (A is in cm^3 sec^{-1}, while E_a is in kcal mol^{-1}). On the other hand, for the monomer reaction, RRHO and VPT2 gave fits of $1.20 \times 10^{-14}\exp(-2.16/RT)$ and $1.24 \times 10^{-14}\exp(-2.08/RT)$, respectively. In accord with the energetics given in Table 1, the water monomer rates increase with temperature while the water dimer rates decrease. The values obtained for the activation energy E_a of the dimer reaction from

the VPT2 and VPT2+HR calculations, are in good agreement with the experimental value[33,34] of 8.3±0.5 kcal mol^{-1} (See ESI for more details). From the VPT2 calculation, we obtain 298 K rate coefficients of 5.44×10^{-12} and 3.69×10^{-16} cm^3 sec^{-1} for the water dimer and monomer reactions, respectively. The room-temperature dimer rate coefficient compares well with the experimental value reported recently, 7.4×10^{-12} cm^3 sec^{-1}.[33] Furthermore, our room temperature monomer rate coefficient is also in agreement with the value reported by Berndt et al.,[24] 3.2×10^{-16} cm^3 sec^{-1}.

One can notice that the RRHO approximation overestimates the rate by a factor of 2 compared to the experimental rates for the dimer reaction. For water clusters, anharmonicities play an important role in obtaining the accurate vibrational spectra.[63] We found that by treating the partition function with VPT2 frequencies, the rate coefficients become nearly one half of those of the RRHO scheme and the VPT2 results reproduce the experimental results for a wide range of temperature. For floppy systems such as water dimer, it is well known that internal hindered rotation of water molecules can play an important role in the calculation of partition functions.[64] In the CI+$(H_2O)_2$ system, we considered two hindered rotors (HRs): (1) the free OH bond (the OH bond that is not forming a hydrogen bond) of H_2O near the OO terminal; and (2) the free OH bond of H_2O at the carbon side. In our approximation, we removed two vibrations corresponding to the HRs and treated each HR as an independent 1-dimensional (1-D) HR[53]. The details in determining the HR potential energy curves are given in the ESI. As shown in Figure 5, the additional correction by the HR treatment further lowers the rate coefficients, which deviates more from the experimental results compared to the pure VPT2 results. We think that using two independent 1-D HRs instead of a coupled 2-D HRs is the possible reason for this discrepancy. Lastly, we comment on the quantum chemistry method dependence of the rate coefficients. As given in the ESI, the use of QCISD(T)/aug-cc-pVTZ or B3LYP/6-311+G(2d,2p) energetics with the VPT2

approach give rate coefficients that are one order of magnitude greater than the experimental results. As conclusion, we have shown that the different methods used for the partition function calculation result in a variation of a factor of 2 in the rate coefficient, and those calculated with QCISD(T)/CBS//B3LYP/6-311+G(2d,2p) energies with VPT2-corrected partition functions gave the best agreement with the experimental values for the CH_2OO reaction.

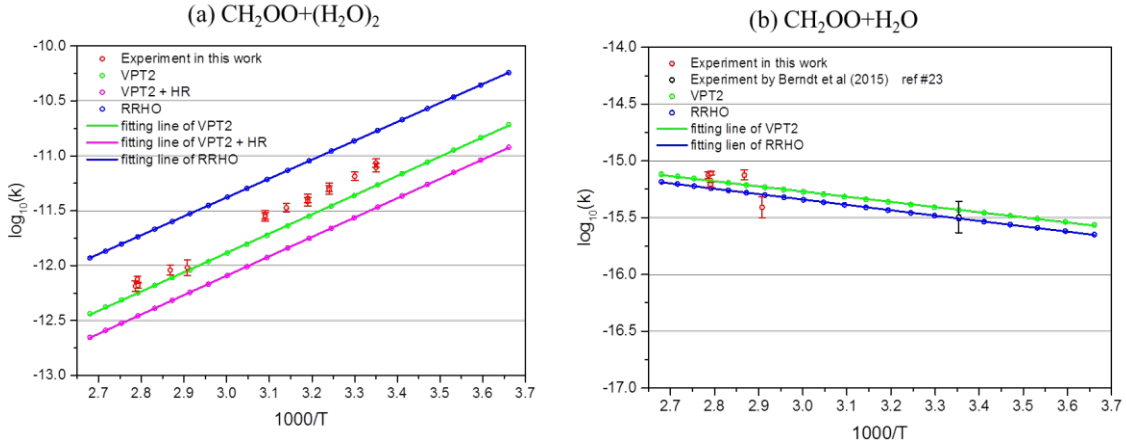

Fig. 5 Arrhenius plot of the (a) $CH_2OO+(H_2O)_2$ rate coefficients in units of cm^3 sec^{-1} by three different methods: RRHO, VPT2, and VPT2+HR; and (b)CH_2OO+H_2O rate coefficients by two methods: RRHO and VPT2. In (a) and (b) our experimental values (this work and Ref. 34) are given with red dots and error bars. In (b) black dot and error bar are presented for experimental values from ref 24.

4. Bimolecular reaction rate of CH_3CHOO with water and water dimer

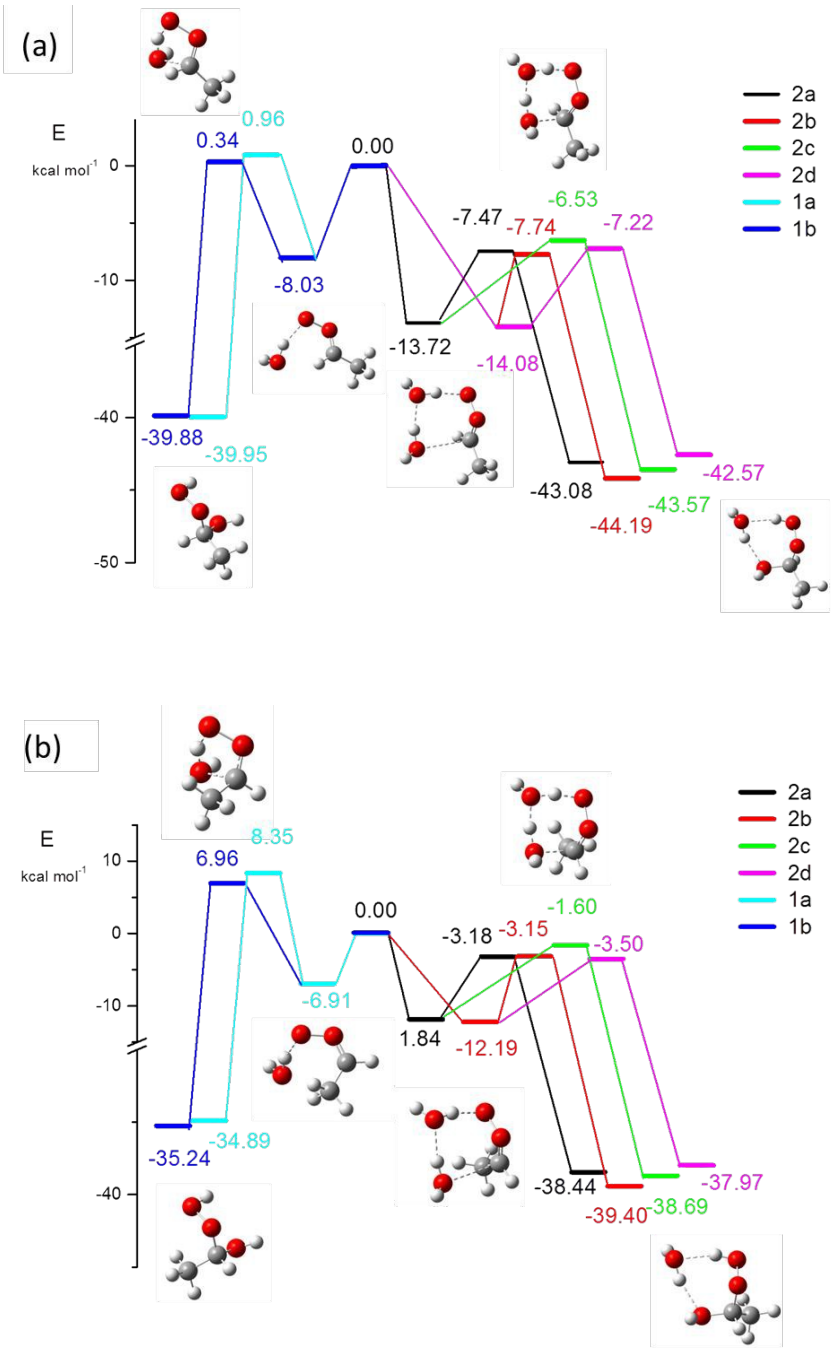

Fig. 6 Potential energy diagram for the reactions of water monomer and dimer with (a) anti-CH_3CHOO and (b) syn-CH_3CHOO. Energetics are calculated using the electronic energies by QCISD(T)/CBS//B3LYP/6-311+G(2d,2p), and vibrational zero-point correction by B3LYP/6-311+G(2d,2p).

In Fig 6, we present the energetics of the *anti*-/*syn*-CH_3CHOO systems. Compared to the CH_2OO system given in Fig 4, one can notice that the formation energy for the VDW complex of *anti*-CH_3CHOO has increased by 1.5 and 3.1 kcal mol^{-1} (average of different pathways) for H_2O and $(H_2O)_2$. On the other hand, due to the steric repulsion of having a methyl group in the same side as the oxygen, the complex formation energy is much smaller for *syn*-CH_3CHOO. For the water monomer 1b reaction, the barrier energy, difference between TS and VDW minima, for *anti*-CH_3CHOO is 8.4 kcal mol^{-1}, which is smaller than the corresponding value 9.4 kcal mol^{-1} for CH_2OO. As a result, for *anti*-$CH_3CHOO+H_2O$, the reaction barrier is nearly isoenergetic with the reactant. When one compares the water dimer reactions of the different CIs, for *anti*-CH_3CHOO, the barrier energy is 6.7 kcal mol^{-1} (average of 4 paths) which is 2.1 kcal mol^{-1} (average of 4 paths) greater than the case for CH_2OO. However, due to the strong VDW complex formation energy, the TS energy with respect to the reactants is 1 kcal mol^{-1} (average of 4 pathways) lower for *anti*-CH_3CHOO compared to CH_2OO. On the other hand, for *syn*-CH_3CHOO, the relative location of the TS energies compared to the reactants are much higher, signifying that it will have much small rate than *anti*-CH_3CHOO or CH_2OO.

The Arrhenius plots for the bimolecular rate coefficients of the water monomer and dimer reactions with *anti*-CH_3CHOO and *syn*-CH_3CHOO are given in Figure 7. Here we used the partition function obtained from the VPT2 approximation since it showed good agreement for CH_2OO. Furthermore compared to the available experimental infrared spectra peak positions for CH_3CHOO[9], VPT2 gave smaller average errors, 32 cm^{-1}, than those obtained from the harmonic approximation, 60 cm^{-1}. To ease the comparison, we also placed the VPT2 results for CH_2OO, as well as the fit to $A\exp(-E_a/RT)$. One can notice that the 298 K bimolecular rate coefficient for the *anti*-CH_3CHOO water monomer reaction is nearly two orders of magnitude larger than that of

CH_2OO. Our theoretical value at 298 K for the *anti*- and *syn*-CH_3CHOO + H_2O reaction is 3.40×10^{-14} and 1.98×10^{-19} cm^3 sec^{-1}, respectively. While the reaction rate coefficients with water dimer are 1.60×10^{-11} and 2.56×10^{-14} cm^3 sec^{-1}, for the *anti*- and *syn*-conformers, respectively. Our present values are an order of magnitude greater than those estimated by Ariya's group[28], but our values are an order of magnitude smaller than the water monomer rate coefficients reported by Anglada's group. Compared to the available experimental values, the *anti*-CH_3CHOO+H_2O rate coefficient is consistent with the recent experimental value of 2.4×10^{-14} cm^3 sec^{-1} by Sheps et al[12]. When compared to the theoretical rate for CH_2OO+H_2O, 3.69×10^{-16} cm^3 sec^{-1}, reported in the previous section, the monomer rate has increased by two orders of magnitude by the addition of methyl group in the *anti*-position of the oxygen. On the other hand, the *anti*-CH_3CHOO+$(H_2O)_2$ reaction rate has only increased by a factor of 3 compared to CH_2OO+$(H_2O)_2$, 5.44×10^{-12} cm^3 sec^{-1}. For the *syn*-conformer, both the water monomer and dimer rate coefficients are three orders of magnitude smaller than those for CH_2OO, and these rates are consistent with the previous experimental report that the *syn*-CH_3CHOO water monomer rate is smaller than 10^{-15} cm^3 sec^{-1}.[7] This is also in line with the previous report that the *anti*-conformer is 3 to 4 orders of magnitude more reactive compared to the *syn*-conformer for the CI reaction with alkenes as well as ozone.[16] From the Arrhenius fit to the VPT2 rate coefficients in cm^3 sec^{-1}, we obtained expressions of $1.63 \times 10^{-18}\exp(9.54/RT)$ and $1.16 \times 10^{-18}\exp(5.93/RT)$ for the water dimer reactions with *anti*- and *syn*-CH_3CHOO, respectively. For the water monomer reactions, we obtained $4.99 \times 10^{-15}\exp(1.14/RT)$ and $3.14 \times 10^{-15}\exp(-5.72/RT)$ for *anti*- and *syn*-CH_3CHOO, respectively.

Lastly, we mention possible errors that have not been considered up to now. First, in the present calculation we assumed thermal equilibrium and used the transition state theory method. Previous studies on complex forming reactions have mentioned the importance of the pressure

dependence and the Master equation should be used to obtain rates.[13] For the CH_2OO experiment, we did not see much pressure dependence so we believe that the assumption of using high pressure limit and thermal equilibrium is valid. Second, the tunneling coefficients were calculated using the semicalssical approximation of Miller et al. which only requires the information at the TS. More sophisticated methods such as the small curvature approximation of Truhlar's group[65,66] may change the results, especially for the hydrogen transfer reaction considered in this study. Although the present reaction involves a hydrogen transfer reaction, the imaginary frequency at the TS was 300i to 500i cm^{-1}. This is much smaller than usual hydrogen transfer reactions which are above 1000 cm^{-1}. Therefore, we believe the barrier is wide enough that the tunneling effect will be small. Indeed, the tunneling correction at 298 K using Miller's semiclassical approach for $CH_2OO+(H_2O)_2$ 2a reaction is only 1.19. Third, this study used usual transition state approximation rather than its variational variant[67,68]. However, we believe that the error of 0.5 kcal mol^{-1} in the quantum chemistry calculations, will wash out any effect of the variational search of the TS. All in all, we think that the uncertainty of 0.5 kcal mol^{-1} in the energetics will give an error about a factor of 2 while the differences in the treatment of the hindered rotors will give an error less than a factor of 2. As conclusion, these contributions will result in total error of factor of ~3 and they are shown as shades in Figure 7.

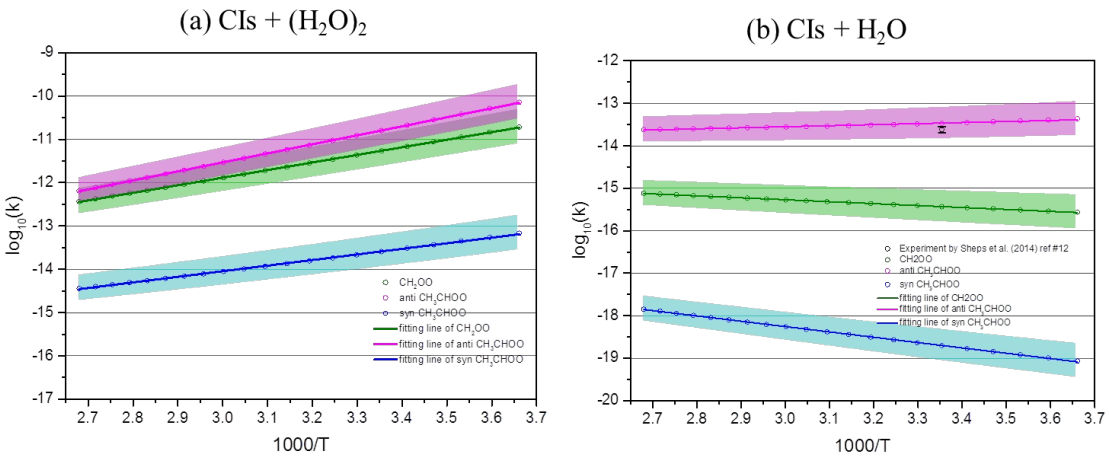

Fig. 7 Arrhenius plots of the CH_2OO, *anti*- and *syn*-CH_3CHOO reaction rate coefficients in cm^3 sec^{-1}, with (7a) $(H_2O)_2$ and (7b) H_2O. Shaded regions show our estimated errors. The available experimental value from ref 12 is given as a black dot.

5. Water concentration and temperature dependence of the effective rate coefficients of CH_2OO/CH_3CHOO reactions with water vapor

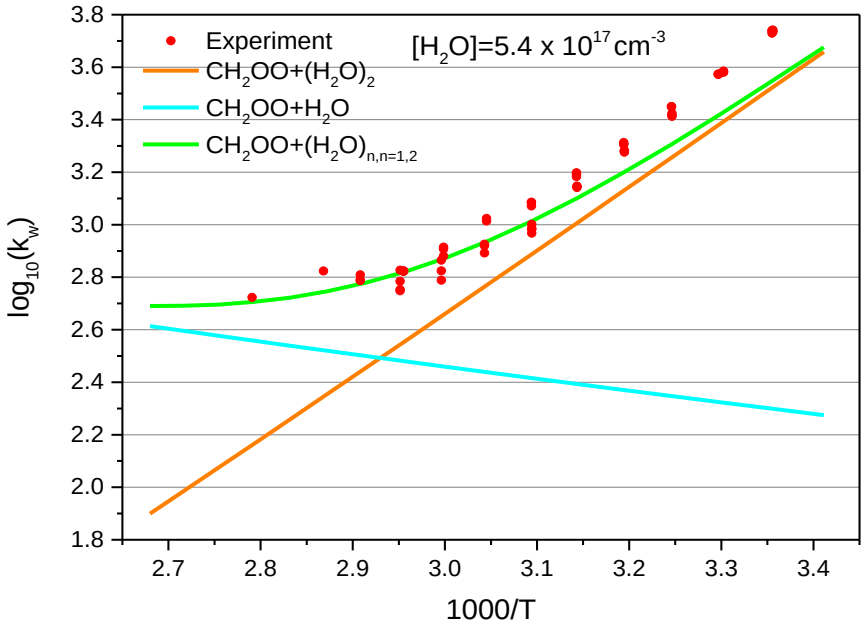

Fig. 8 Effective first-order rate coefficients in sec^{-1} for $CH_2OO+(H_2O)_2$ (orange) and CH_2OO+H_2O reaction (light blue); and their summed contribution $[CH_2OO+(H_2O)_n$, n=1,2] (light green). The

red dots represent our experimental values (this work and Ref. 33). This plot is made for $[H_2O]=5.4\times10^{17}$ molecule cm^{-3}.

At the water concentration used in the experiment, $[H_2O]=5.4\times10^{17}$ molecules cm^{-3}, we perform a direct comparison of the experiment and theoretical effective rates. In Figure 8, we present the temperature dependence of the effective rate coefficient for CH_2OO (light green) reaction with water vapor and their water monomer contribution $\sum_i k_{mono,i}[H_2O]$ (light blue) and water dimer contribution $\sum_j k_{dimer,j}[(H_2O)_2]$ (orange). Consistent with the values given in Figure 5, the effective rate coefficients also show good agreement with the experimental values. As can be expected from the opposing trends of the H_2O and $(H_2O)_2$ reactions, the water monomer reaction which can be ignored at room temperature becomes important at higher temperatures. This causes the negative temperature dependence of the theoretical effective rate of CH_2OO reaction with water vapor to level off at temperatures greater than 333K. This feature is also observed at similar temperatures in the experimental rate constant.

Next we examine how this trend changes with the substitution of the methyl group. In Figure 9, we compare the effective rate coefficients of CH_2OO, *anti*-CH_3CHOO, and *syn*-CH_3CHOO at $[H_2O]=5.4\times10^{17}$ molecule cm^{-3}. As mentioned in the previous sections, our bimolecular rate coefficients may have an error of a factor of 3. Therefore, we compare our best estimated values as well as those obtained by the upper and lower limits in Figure 9. As can be seen from these plots, the general trend in the temperature dependence is very sensitive to the relative values of the monomer and dimer rate coefficients. However, all estimates show that at room temperature the effective rates for the CH_2OO, *anti*-CH_3CHOO and *syn*-CH_3CHOO at $[H_2O]\sim5\times10^{17}$ cm^{-3} will be $\sim10^3$, $\sim10^4$, and $\sim10^1$ s^{-1}, respectively. In atmospheric conditions, the water number density may vary between 1×10^{17} to 5×10^{17} cm^{-3}, and as seen in the plots for $[H_2O]=$

1×10^{17} and 2×10^{17} cm^{-3} in the Figure S10 in ESI, the general time scale of the CI reaction with water vapor does not vary that greatly.

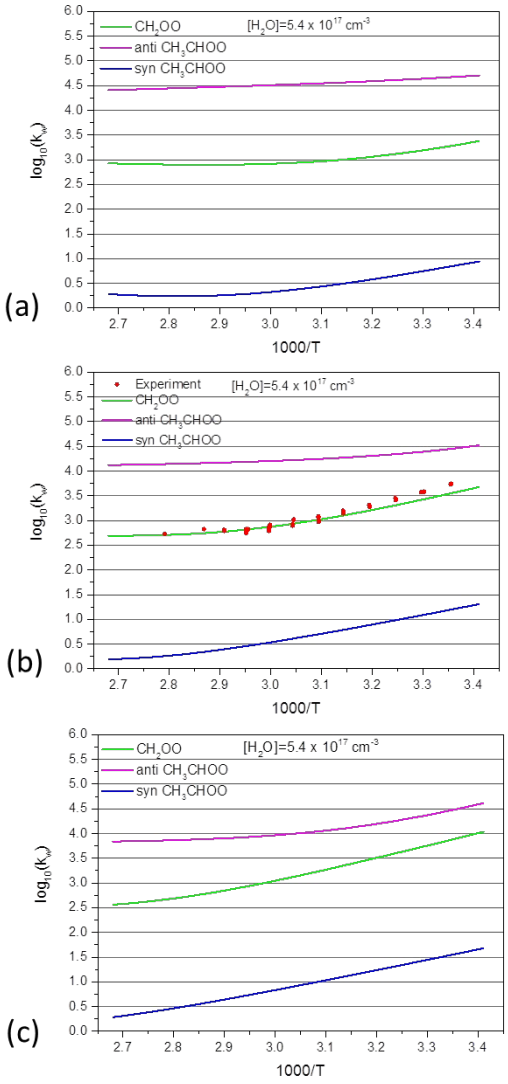

Fig 9. The Arrhenius plots of the effective first-order rate coefficients in unit of sec^{-1}. (a) Calculated using the lower and upper bounds for the CIs+$(H_2O)_2$ and CIs+H_2O bimolecular rate coefficients, respectively. (b) Calculated using best estimates for the CIs+$(H_2O)_2$ and CIs+H_2O bimolecular rate coefficients. The red dots represent our experiment data. (c) Calculated using the upper and lower bounds for the CIs+$(H_2O)_2$ and CIs+H_2O bimolecular rate coefficients, respectively. The rate coefficients were calculated with VPT2 scheme and energies from QCISD(T)/CBS//B3LYP/6-311+G(2d,2p). The green, magenta, and blue lines represent the water vapor reactions of CH_2OO, *anti*-CH_3CHOO, and *syn*-CH_3CHOO, respectively. These plots are for $[H_2O]=5.4\times10^{17}$ cm^{-3}.

Conclusion and atmospheric implications

In this study, we extended our previous experimental study to higher temperatures and obtained the rate coefficient of CH_2OO+H_2O to be 7.3×10^{-16} cm^3 sec^{-1} at 358 K. We confirmed the negative temperature dependence of the CI water vapor reaction at a wide range of temperatures using theoretical and experimental investigations. Theoretically we showed that the water dimer bimolecular reaction is responsible for the negative temperature dependence. On the other hand, we calculated that the water monomer bimolecular rate coefficient, which is four orders smaller compared to the water dimer rate coefficient for CH_2OO at room temperature, increases with temperature. This competing effect of the monomer and dimer rate coefficients, and the decrease of water dimer population at high temperature causes the negative temperature dependence of the effective rate to level off at 333 K for $[H_2O]=5.4\times10^{17}$ cm^{-3}.

Furthermore, using the same methodology we calculated rate coefficients for *anti*-/*syn*-CH_3CHOO reactions with water vapor. For the more reactive *anti*-conformer, we obtained bimolecular rate coefficients of 1.60×10^{-11} and 3.40×10^{-14} cm^3 sec^{-1} for $(H_2O)_2$ and H_2O reactions at room temperature. These values are much larger than the corresponding values of 5.44×10^{-12} and 3.69×10^{-16} cm^3 sec^{-1} for CH_2OO and 2.56×10^{-14} and 1.98×10^{-19} cm^3 sec^{-1} for *syn*-CH_3CHOO. From the detailed analysis on the energetics and calculation method of the rate constants, we believe that our theoretical estimates are within a factor of 3 of the real value. At atmospherically relevant water concentrations, the effective rate coefficients for the CH_2OO, *anti*-CH_3CHOO and *syn*-CH_3CHOO reactions with water vapor will be ~10^3, ~10^4, and ~10^1 s^{-1}, respectively, at room temperature. Therefore, it is likely that water will react with CH_2OO and *anti*-CH_3CHOO faster than these CIs can actively participate as an oxidant of SO_2 or NO_2 in the atmosphere. Here we have shown that the substitution of a methyl group in the *anti*-position of the terminal oxygen atom

causes the effective rate coefficient to increase by 10 times compared to CH_2OO at atmospherically relevant water concentrations. However in order to understand atmospherically relevant CIs, we should extend the study to CIs of longer chains.[69] This study showed that simulation using VPT2 calculation and high level quantum chemistry calculation can obtain rate coefficients which agree with the experimental results for a wide range of temperatures. Thereby, we think this simulation method can be used to assess the temperature dependent rate for CI with longer alkyl chains which are relevant in atmospheric studies and research along that direction is presently pursued.

On the other hand, the very slow rates for the *syn*-CH_3CHOO water reaction state that it will likely participate in the SO_2 oxidation process. Indeed, recent measurements on $(CH_3)_2COO$ have shown that conformers with a methyl group in the *syn*-position of the OO bond can actively react with SO_2 even under humid conditions.[70] Here we note that when considering the atmospheric fate of the CIs, the decomposition of the stabilized CI will also compete with the water reaction. Previous theoretical studies have shown that conformers with alkyl groups in the *syn*-position of the oxygen will decompose faster than those with alkyl groups in the *anti*-position.[13,32] Therefore, accurate rate coefficients for this process is also presently being pursued both experimentally and theoretically.

Considering the large exothermicity, ~40 kcal mol^{-1}, of the reaction between CIs and water vapor, it is important to know how these hot hydroxyalkyl hydroperoxide products decompose. Previous study by Anglada et al.[30] has mentioned efficient production of OH radicals which can act as an oxidizing agent in the atmosphere. However, ozonolysis experiments have not seen clear correlation between OH production and humidity.[71–73] To gain understanding on the consequences from the fast CI water reactions in the atmosphere, we think that the direct detection of the products of CI reaction with H_2O and $(H_2O)_2$ is also necessary.

ELECTRONIC SUPPLEMENTARY MATERIAL

Electronic Supplementary Information (ESI) available: Details concerning the estimate of the water concentration error and experimental conditions for the high temperature experiments; details of the quantum chemistry energetics, geometries obtained by QCISD(T) method, values of the rate coefficients; discussion on the hindered rotor approximation, and discussion on effective rates as well as discussion on the water dimer equilibrium constants.

Notes

The authors declare no competing financial interests.

ACKNOWLEDGMENT

This research was supported by Academia Sinica and the Ministry of Science and Technology of Taiwan (MOST103-2113-M-001-019-MY3; 102-2113-M-001-012-MY3).

REFERENCES

1 R. Criegee, *Angew. Chem. Int. Ed.*, 1975, **14**, 745–752.

2 R. L. Mauldin III, T. Berndt, M. Sipilä, P. Paasonen, T. Petäjä, S. Kim, T. Kurtén, F. Stratmann, V.-M. Kerminen and M. Kulmala, *Nature*, 2012, **488**, 193–196.

3 C. A. Taatjes, D. E. Shallcross and C. J. Percival, *Phys. Chem. Chem. Phys.*, 2014, **16**, 1704–18.

4 Y.-P. Lee, *J. Chem. Phys.*, 2015, **143**, 020901.

5 C. A. Taatjes, G. Meloni, T. M. Selby, A. J. Trevitt, D. L. Osborn, C. J. Percival and D. E. Shallcross, *J Am Chem Soc*, 2008, **130**, 11883–11885.

6 O. Weltz, J. D. Savee, D. L. Osborn, S. S. Vasu, C. J. Percival, D. E. Shallcross and C. A. Taatjes, *Science*, 2012, **335**, 204–207.

7 C. A. Taatjes, O. Welz, A. J. Eskola, J. D. Savee, A. M. Scheer, D. E. Shallcross, B. Rotavera, E. P. F. Lee, J. M. Dyke, D. K. W. Mok, D. L. Osborn and C. J. Percival, *Science*, 2014, **340**, 177.

8 O. Welz, A. J. Eskola, L. Sheps, B. Rotavera, J. D. Savee, A. M. Scheer, D. L. Osborn, D. Lowe, A. Murray Booth, P. Xiao, M. A. H. Khan, C. J. Percival, D. E. Shallcross and C. A. Taatjes, *Angew. Chemie - Int. Ed.*, 2014, **53**, 4547–4550.

9 H.-Y. Lin, Y.-H. Huang, X. Wang, J. M. Bowman, Y. Nishimura, H. A. Witek and Y.-P. Lee, *Nat. Commun.*, 2015, **6**, 7012.

10 R. Chhantyal-Pun, A. Davey, D. E. Shallcross, C. J. Percival and A. J. Orr-Ewing, *Phys. Chem. Chem. Phys.*, 2015, **17**, 3617–3626.

11 D. Stone, M. Blitz, L. Daubney, N. U. M. Howes and P. Seakins, *Phys. Chem. Chem. Phys.*, 2014, **16**, 1139–1149.

12 L. Sheps, A. M. Scully and K. Au, *Phys. Chem. Chem. Phys.*, 2014, **16**, 26701–26706.

13 K. T. Kuwata, M. R. Hermes, M. J. Carlson and C. K. Zogg, *J. Phys. Chem. A*, 2010, **114**, 9192–9204.

14 L. Vereecken and J. S. Francisco, *Chem. Soc. Rev.*, 2012, **41**, 6259–6293.

15 L. Vereecken, H. Harder and A. Novelli, *Phys. Chem. Chem. Phys.*, 2012, **14**, 14682–14695.

16 L. Vereecken, H. Harder and A. Novelli, *Phys. Chem. Chem. Phys.*, 2014, **16**, 4039–4049.

17 M. Kumar, D. H. Busch and W. H. Thompson, *Phys. Chem. Chem. Phys.*, 2014, **16**, 22968–22973.

18 H. G. Kjaergaard, T. Kurtén, L. B. Nielsen, S. Jørgensen and P. O. Wennberg, *J. Phys. Chem. Lett.*, 2013, **4**, 2525–2529.

19 G. Sarwar, H. Simon, K. Fahey, R. Mathur, W. S. Goliff and W. R. Stockwell, *Atmos. Environ.*, 2014, **85**, 204–214.

20 C. J. Percival, O. Welz, A. J. Eskola, J. D. Savee, D. L. Osborn, D. O. Topping, D. Lowe, S. R. Utembe, A. Bacak, G. McFiggans, M. C. Cooke, P. Xiao, A. T. Archibald†, M. E. Jenkin, R. G. Derwent, I. Riipinen, D. W. K. Mok, E. P. F. Lee, J. M. Dyke, C. A. Taatjes and D. E. Shallcross, *Faraday Discuss.*, 2013, **165**, 45–73.

21 S. Hatakeyama, H. Bandow, M. Okuda and H. Akimoto, *J. Phys. Chem.*, 1981, **85**, 2249–2254.

22 P. Neeb, F. Sauer, O. Horie and G. K. Moortgat, *Atmos. Environ.*, 1997, **31**, 1417–1423.

23 T. Berndt, J. Voigtländer, F. Stratmann, H. Junninen, R. L. Mauldin, M. Sipilä, M. Kulmala and H. Herrmann, *Phys. Chem. Chem. Phys.*, 2014, **16**, 19130–19136.

24 T. Berndt, R. Kaethner, J. Voigtländer, F. Stratmann, M. Pfeifle, P. Reichle, M. Sipilä, M. Kulmala and M. Olzmann, *Phys. Chem. Chem. Phys.*, 2015, **17**, 19862–19873.

25 B. Ouyang, M. M. W., R. L. Jones and W. L. Bloss, *Phys. Chem. Chem. Phys.*, 2013, **15**, 17070–17075.

26 A. B. Ryzhkov and P. A. Ariya, *Chem Phys Lett*, 2003, **367**, 423–429.

27 A. B. Ryzhkov and P. A. Ariya, *Phys. Chem. Chem. Phys.*, 2004, **6**, 5042–5050.

28 A. B. Ryzhkov and P. A. Ariya, *Chem Phys Lett*, 2006, **419**, 479–485.

29 R. Crehuet, J. M. Anglada and J. M. Bofill, *Chem. Eur. J.*, 2001, **7**, 2227–2235.

30 J. M. Anglada, P. Aplincourt, J. M. Bofill and D. Cremer, *Chem. Phys. Chem.*, 2002, 215–221.

31 P. Aplincourt and J. M. Anglada, *J. Phys. Chem. A*, 2003, **107**, 5798–5811.

32 J. M. Anglada, J. González and M. Torrent-sucarrat, *Phys. Chem. Chem. Phys.*, 2011, **13**, 13034–13045.

33 W. Chao, J. Hsieh, C. Chang and J. J. Lin, *Science*, 2015, **347**, 751–754.

34 M. C. Smith, C.-H. Chang, W. Chao, L.-C. Lin, K. Takahashi, K. A. Boering and J. J.-M. Lin, *J. Phys. Chem. Lett.*, 2015, **6**, 2708–2713.

35 A. Becke, *J. Chem. Phys.*, 1993, **98**, 5648–5652.

36 C. Lee, W. Yang and R. G. Parr, *Phys. Rev. B*, 1988, **37**, 785–789.

37 R. Krishnan, J. S. Binkley, R. Seeger and J. A. Pople, *J. Chem. Phys.*, 1980, **72**, 650.

38 M. J. Frisch, J. A. Pople and J. S. Binkley, *J. Chem. Phys.*, 1984, **80**, 3265.

39 V. Barone, *J. Chem. Phys.*, 2005, **122**, 1–10.

40 V. Barone, M. Biczysko and J. Bloino, *Phys. Chem. Chem. Phys.*, 2013, **16**, 1759–87.

41 Gaussian09, M. J. Frisch, G. W. Trucks, H. B. Schlegel, G. E. Scuseria, M. A. Robb, J. R. Cheeseman, G. Scalmani, V. Barone, B. Mennucci, G. A. Petersson, H. Nakatsuji, M. Caricato, X. Li, H. P. Hratchian, A. F. Izmaylov, J. Bloino, G. Zheng, J. L. Sonnenberg, M. Hada, M. Ehara, K. Toyota, R. Fukuda, J. Hasegawa, M. Ishida, T. Nakajima, Y. Honda, O. Kitao, H. Nakai, T. Vreven, J. Montgomery, J. A., J. E. Peralta, F. Ogliaro, M. Bearpark, J. J. Heyd, E. Brothers, K. N. Kudin, V. N. Staroverov, R. Kobayashi, J. Normand, K. Raghavachari, A. Rendell, J. C. Burant, S. S. Iyengar, J. Tomasi, M. Cossi, N. Rega, J. M. Millam, M. Klene, J. E. Knox, J. B. Cross, V. Bakken, C. Adamo, J. Jaramillo, R. Gomperts, R. E. Stratmann, O. Yazyev, A. J. Austin, R. Cammi, C. Pomelli, J. W. Ochterski, R. L. Martin, K. Morokuma, V. G. Zakrzewski, G. A. Voth, P. Salvador, J. J. Dannenberg, S. Dapprich, A. D. Daniels, Ö. Farkas, J. B. Foresman, J. V. Ortiz, J. Cioslowski and D. J. Fox, 2009.

42 K. A. Peterson, D. E. Woon and T. H. Dunning, *J. Chem. Phys.*, 1994, **100**, 7410–7415.

43 T. H. Dunning, *J. Chem. Phys.*, 1989, **90**, 1007–1023.

44 R. A. Kendall, T. H. Dunning and R. J. Harrison, *J Chem Phys*, 1992, **96**, 6796–6806.

45 J. Dunning T.H., K. A. Peterson and A. K. Wilson, *J. Chem. Phys.*, 2001, **114**, 9244–9253.

46 J. A. Pople, M. Head-Gordon and K. Raghavachari, *J. Chem. Phys.*, 1987, **87**, 5968–5975.

47 K. Raghavachari, G. W. Trucks, J. A. Pople and M. Head-Gordon, *Chem. Phys. Lett.*, 1989, **179**, 479–483.

48 MOLPRO, H.-J. Werner, P. J. Knowles, F. R. Manby, M. Schütz, P. Celani, G. Knizia, T. Korona, R. Lindh, A. Mitrushenkov, G. Rauhut, T. B. Adler, R. D. Amos, A. Bernhardsson, A. Berning, D. L. Cooper, M. J. O. Deegan, A. J. Dobbyn, F. Eckert, E. Goll, C. Hampel, A. Hesselmann, G. Hetzer, T. Hrenar, G. Jansen, C. Köppl, Y. Liu, A. W. Lloyd, R. A. Mata, A. J. May, S. J. McNicholas, W. Meyer, M. E. Mura, A. Nicklaß,

P. Palmieri, K. Pflüger, R. Pitzer, M. Reiher, T. Shiozaki, H. Stoll, A. J. Stone, R. Tarroni, T. Thorsteinsson, M. Wang and A. Wolf, 2011.

49 B. Ruscic, *J. Phys. Chem. A*, 2013, **117**, 11940–11953.

50 W. H. Miller, R. Hernandez, N. C. Handy, D. Jayatilaka and A. Willetts, *Chem. Phys. Lett.*, 1990, **172**, 62–68.

51 M. J. Cohen, N. C. Handy, R. Hernandez and W. H. Miller, *Chem. Phys. Lett.*, 1992, **192**, 407–416.

52 J. R. Barker, *Int. J. Chem. Kinet.*, 2000, 232.

53 T. L. Nguyen and J. R. Barker, *J. Phys. Chem. A*, 2010, **114**, 3718–3730.

54 M. Basire, P. Parneix and F. Calvo, *J Chem Phys*, 2008, **129**, 081101.

55 Multiwell-2104.1, J. R. Barker, N. F. Ortiz, J. M. Preses, L. L. Lohr, A. Maranzana, P. J. Stimac, T. L. Nguyen and T. J. Dhilip Kumar, 2014.

56 M. Nakajima and Y. Endo, *J. Chem. Phys.*, 2014, **140**, 134302.

57 L. B. Harding and W. A. Goddard, *J. Am. Chem. Soc.*, 1978, **100**, 7180–7188.

58 W. R. Wadt and W. A. Goddard, *J. Am. Chem. Soc.*, 1975, **97**, 3004–3021.

59 D. Cremer, *J. Am. Chem. Soc.*, 1979, **101**, 7199–7205.

60 T. J. Lee and P. R. Taylor, *Int. J. Quantum Chem. Quant. Chem. Sym.*, 1989, **23**, 199–207.

61 J. M. Anglada, S. Olivella and A. Sole, *Phys. Chem. Chem. Phys.*, 2013, **15**, 18921–18933.

62 E. Miliordos, K. Ruedenberg and S. S. Xantheas, *Angew. Chemie - Int. Ed.*, 2013, **52**, 5736–5739.

63 B. Temelso and G. C. Shields, *J Chem Theo Comput*, 2011, **7**, 2804–2817.

64 C. Leforestier, *J Chem Phys*, 2014, **140**, 74106.

65 R. T. Skodje, D. G. Truhlar and B. C. Garrett, *J. Phys. Chem.*, 1981, **85**, 3019–3023.

66 R. T. Skodje, D. G. Truhlar and B. C. Garrett, *J. Chem. Phys.*, 1982, **77**, 5955–5976.

67 D. G. Truhlar, B. C. Garrett and S. J. Klippenstein, *J. Phys. Chem.*, 1996, **100**, 12771–12800.

68 D. G. Truhlar and B. C. Garrett, *Annu. Rev. Phys. Chem.*, 1984, **35**, 159–189.

69 M. J. Newland, a. R. Rickard, L. Vereecken, a. Muñoz, M. Ródenas and W. J. Bloss, *Atmos. Chem. Phys.*, 2015, **15**, 9521–9536.

70 H.-L. Huang, W. Chao and J. J.-M. Lin, *Proc. Natl. Acad. Sci.*, 2015, 201513149.

71 H. Berresheim, M. Adam, C. Monahan, C. O'Dowd, J. M. C. Plane, B. Bohn and F. Rohrer, *Atmos. Chem. Phys. Discuss.*, 2014, **14**, 1159–1190.

72 R. Tillmann, M. Hallquist, Å. M. Jonsson, a. Kiendler-Scharr, H. Saathoff, Y. Iinuma and T. F. Mentel, *Atmos. Chem. Phys.*, 2010, **10**, 7057–7072.

73 R. M. Harrison, J. Yin, R. M. Tilling, X. Cai, P. W. Seakins, J. R. Hopkins, D. L. Lansley, a. C. Lewis, M. C. Hunter, D. E. Heard, L. J. Carpenter, D. J. Creasey, J. D. Lee, M. J.

Pilling, N. Carslaw, K. M. Emmerson, a. Redington, R. G. Derwent, D. Ryall, G. Mills and S. a. Penkett, *Sci. Total Environ.*, 2006, **360**, 5–25.